Available online at www.sciencedirect.com
ScienceDirect
Trans. Nonferrous Met. Soc. China 27(2017) 110−116
Transactions of Nonferrous Metals Society of China
www.tnmsc.cn

# Beryllium-distribution in metallic glass matrix composite containing beryllium

Zhen-xi GUO[1,2], Yong-sheng WANG[3,4], Lu-jun ZHU[1], Yue-fei ZHANG[1], Zhen-hua ZHANG[1], Xiao-xing KE[1], Jun-pin LIN[4], Guo-jian HAO[4], Ze ZHANG[1,5], Man-ling SUI[1]

1. Institute of Microstructure and Property of Advanced Materials, Beijing University of Technology, Beijing 100124, China;
2. Center for Biological Imaging, Core Facilities for Protein Science, Institute of Biophysics, Chinese Academy of Sciences, Beijing 100101;
3. College of Materials Science and Engineering, Taiyuan University of Technology, Taiyuan 030024, China;
4. State Key Laboratory for Advanced Metals and Materials, University of Science and Technology Beijing, Beijing 100083, China;
5. Department of Materials Science and Engineering, State Key Laboratory of Silicon Materials, Zhejiang University, Hangzhou 310027, China

Received 26 October 2015; accepted 28 September 2016

**Abstract:** The morphologies, sizes, compositions and volume fractions of dendritic phases in in situ Ti-based metallic glass matrix composites (MGMCs) containing beryllium (Be) with the nominal composition of $Ti_{47}Zr_{19}Cu_5V_{12}Be_{17}$ (mole fraction, %) were investigated using XRD, SEM, EBSD, TEM, EDS and three-dimensional reconstruction method. Moreover, visualized at the nanoscale, Be distribution is confirmed to be only present in the matrix using scanning transmission electron microscopy−electron energy loss spectroscopy (STEM−EELS). Based on these findings, it has been obtained that the accurate chemical compositions are $Ti_{28.3}Zr_{19.7}Cu_8V_{6.4}Be_{37.6}$ (mole fraction, %) for glass matrix and $Ti_{62.4}Zr_{18.4}Cu_{2.6}V_{16.6}$ (mole fraction, %) for the dendritic phases, and the volume fractions are 38.5% and 61.5%, respectively. It is believed that the results are of particular importance for the designing of Be-containing MGMCs.

**Key words:** metallic glass; composites; microstructure; electron energy loss spectroscopy; Be-distribution

## 1 Introduction

Metallic glasses (MGs) have attracted great attention due to their unparalleled mechanical properties [1−5] such as high strength, large elastic limit and good wear resistance. However, the lack of global plasticity, caused by the localized shear bands, has limited their engineering applications. Much effort has been put into optimizing the composition and the microstructure of MGs in order to overcome this problem [6−8]. In situ metallic glass matrix composites (MGMCs) [9−13] have been proved to be the efficient way to decrease the brittleness of MGs. It has been found that the precipitated crystalline phase can obstruct the unlimited propagation of the single shear band and promote the formation of multiple shear bands, which improves the global plasticity [9]. Since the first report of Zr-based MGMCs by HAYS et al [9], a number of such materials with varying components have been developed, e.g., Zr-based MGMCs [9−15], and Ti-based MGMCs [16,17].

In particular, Be-containing MGMCs have drawn great attention thanks to their superior mechanical properties [11,9,18], such as high strength and plasticity. Be element, as one of the great important elements to the applications in aerospace and nuclear industries [19], has been confirmed to improve the mechanical properties [20], glass forming ability [21,22] and thermal stability [15] of MGs. Meanwhile, Be element in MGMCs has been proved to improve mechanical properties [14,17] due to its low density and high elastic modulus. Therefore, the analysis of the Be distribution in alloys is of great significance. However, the current

**Foundation item:** Project (11374028) supported by the National Natural Science Foundation of China; Project supported by the Cheung Kong Scholars Program of China
**Corresponding author:** Zhen-xi GUO; Tel:+86-10-64888419; E-mail: guozhenxi9999@ibp.ac.cn
DOI: 10.1016/S1003-6326(17)60012-8

method to characterize the composition distribution in Be-containing MGMCs is mainly limited to energy dispersive X-ray spectroscopy (EDS), which is unfortunately not sensitive to light elements, including Be. While most compositional studies of the Be-containing MGMCs are limited to heavy elements [23], little progress has been made on Be distribution which is crucial for understanding the material. Although previous studies have predicted that Be is partitioned into the glass matrix [9,17], direct investigations of the element distribution have not yet been reported.

In this work, the Be distribution is revealed by using scanning transmission electron microscopy−electron energy loss spectroscopy (STEM−EELS). By further investigating the volume fraction of a dendrite using image quality (IQ) and EDS in scanning electron microscope (SEM), the compositions of the two phases in these Be-containing MGMCs have been quantified.

## 2 Experimental

### 2.1 Sample fabrication

Ingots with the nominal composition of $Ti_{47}Zr_{19}Cu_5V_{12}Be_{17}$ (mole fraction, %) were prepared by arc-melting, a mixture of high purity elements (>99.9%) under an argon atmosphere. Rod-like composite samples were fabricated by Bridgman solidification [24].

### 2.2 Microstructure and composition characterization

The microstructure was characterized by using FEI Quanta 250 SEM. The crystal structure of the samples was analyzed by X-ray diffraction (XRD) using a Cu $K_\alpha$ radiation in Bruker D8 Advance diffractometer. The 3D study of the structure was performed on a dual beam focused ion beam/SEM(FEI Helios NanoLab 600i) via serial-sectioning procedures. The 3D reconstruction was performed by using Amira software. The chemical composition was determined by means of Hitachi S−3400N SEM with X-Flash ® 5030 EDS and the FEI Titan ChemiSTEM equipped with Gatan GIF Quantum 965. The convergent angle and collection semi-angle for STEM−EELS are of 21 mrad and 40 mrad. Electron backscattered diffraction (EBSD) analysis was conducted on JEM−6500F with EDAX-TSL EBSD. During EBSD testing, the electron beam scanned on the sample surface and generated a Kikuchi pattern composed of intersecting Kikuchi bands at each measurement point [25]. The image quality (IQ) parameter describes the quality of the Kikuchi pattern, which is the representative of lattice planes in the diffracting crystal. Thus, the amorphous matrix cannot generate the Kikuchi pattern, and the IQ is close to zero. By means of the IQ, we can get the volume fraction of the dendrites in a more accurate and efficient way. Transmission electron microscopy (TEM) analysis was performed using a JEOL−2010F equipped with a field emission gun operated at 200 kV. The TEM samples were cut from the rod-like composite samples, which were mechanically polished and then ion-milled until perforation at 5 kV using a precision ion polishing system (Gatan model 691PIPS) with a liquid nitrogen cooling system operating at −150 °C.

## 3 Results

Figure 1(a) shows typical SEM backscattered image of the composites. It could be seen that the crystalline phase (dark contrast) is formed and it is uniformly dispersed in the amorphous glassy matrix (bright contrast) throughout the entire cross section. In terms of the composites, XRD shows diffraction peaks from $\beta$-Ti superimposed with the broad diffuse scattering features from the glassy matrix as shown in Fig. 1(b). The volume fraction of the dendrites can be determined from the peak area ratio, which was found to be about 60%. Since the microstructure of a composite is strongly related to its mechanical properties, a statistical study of the dendritic diameter distribution has been performed using TEM images. The dendritic diameter is 0.5−2 μm, as shown in Fig. 1(c). The inter-dendritic distance is about 300 nm, as shown in Fig. 1(d), which is consistent with previous reports [16,17,24]. It is believed that a smaller inter-dendritic distance has a positive influence on the ductility of the glass [4].

The microstructure of the reinforced crystalline phases dispersed in a glassy matrix plays an important role in determining the mechanical properties of a composite. However, current morphological studies mostly rely on two dimensional (2D) images, which are insufficient for the understanding of all features and connections between the dendritic structures. A more comprehensive understanding of the dendritic structure in 3D is therefore desirable in order to provide a direct visualization of the composite. Figure 2(a) shows a snapshot of the dendritic 3D network. A serial snapshot of the 3D structure can be found in the supplementary information. The crystalline phase forms interconnecting dendritic structure which is homogeneously dispersed within the amorphous matrix. The good connectivity of such reticular structures efficiently prevents the rapid expansion of the shear zone. The volume fraction of the dendrites is almost the same in every section.

The volume fraction of the dendrites has an important effect on the performance of the material. This fraction is usually determined by analyzing the contrast in images [26] or by differential scanning calorimetry analysis [27] which may introduce a significant

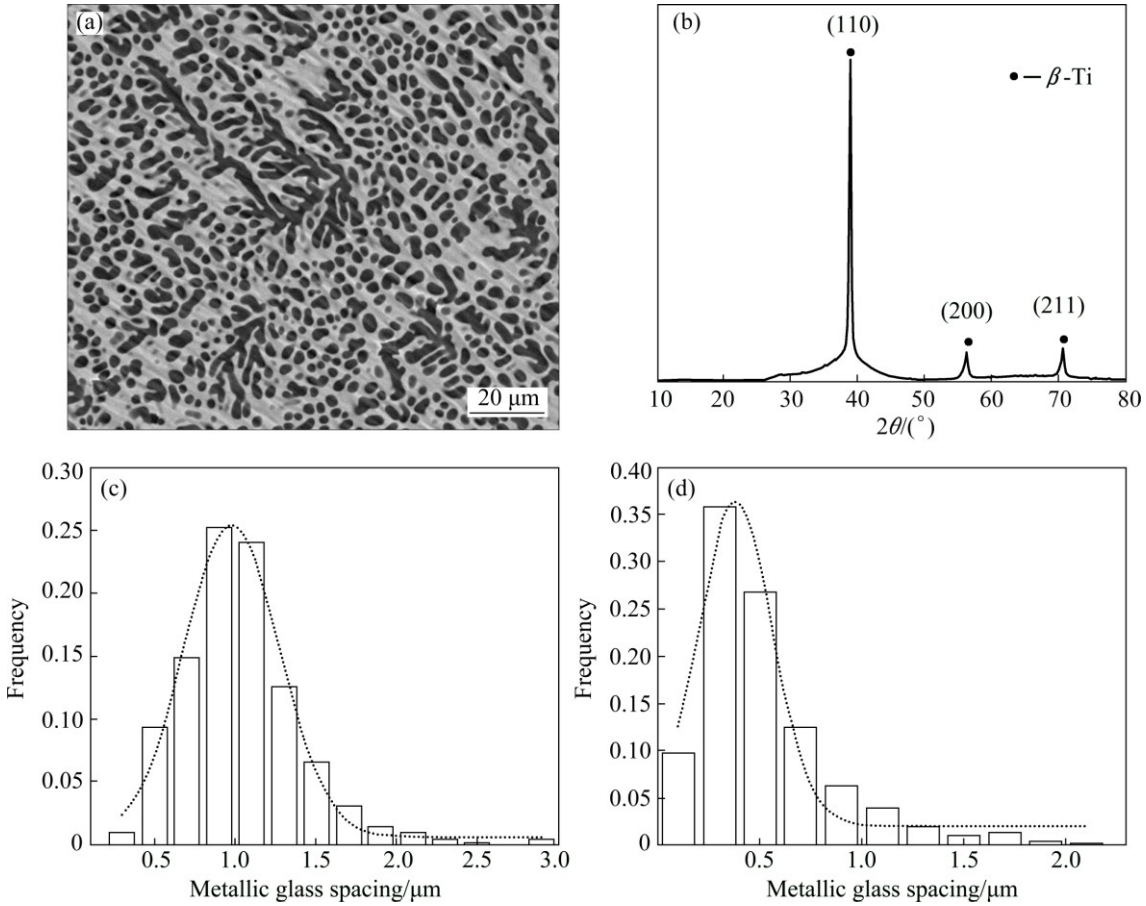


**Fig. 1** SEM backscattered electron micrograph of composite (a), XRD pattern of composite (b), statistical distribution of dendritic diameter (c) and statistical distribution of inter-dendritic spacing (d)

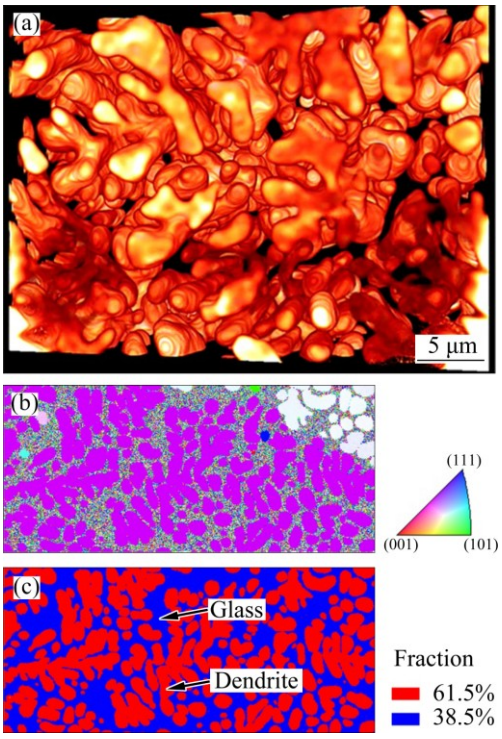


**Fig. 2** 3D reconstruction of interconnecting dendrites (a), IPF color map (b) and IQ map of composites (c)

calculation error. A more precise calculation has been performed by using EBSD data, as shown in Figs. 2(b) and (c). Inverse pole figure color maps mark the orientation of each of the dendritic phases by different colors as shown in Fig. 2(b). The image quality (IQ) parameter distinguishes the amorphous phase and the crystallized phase, and it is used to generate the volume fraction in a more accurate and efficient way. In our alloys, the volume fraction of dendrites was found to be approximately 61.5% based on the IQ as shown in Fig. 2(c). This result is in good agreement with the XRD data shown in Fig. 1(b), which confirms the high volume fraction of the crystallized phase.

To further investigate the alloy structure at higher resolution, TEM study was performed on the composite. Figure 3(a) shows the dendritic phase (white regions) dispersed in the matrix (gray regions). Figure 3(b) shows the selected-area electron diffraction (SAED) pattern obtained from the amorphous matrix, in which no crystallization can be detected. Figure 3(c) shows the SAED pattern taking along the [111] zone axis of one typical dendrite, which confirms the body center cubic structure of the crystalline phase. Since EELS is sensitive to low atomic number elements, STEM−EELS is used to

determine the Be distribution. The background subtracted EELS spectra of the Be-K edge, obtained from the matrix and the dendrites are shown in Fig. 3(d). It is clear that Be is absent in the dendrite (red regions in Fig. 3(d)) but present exclusively in the matrix (black regions in Fig. 3(d)).

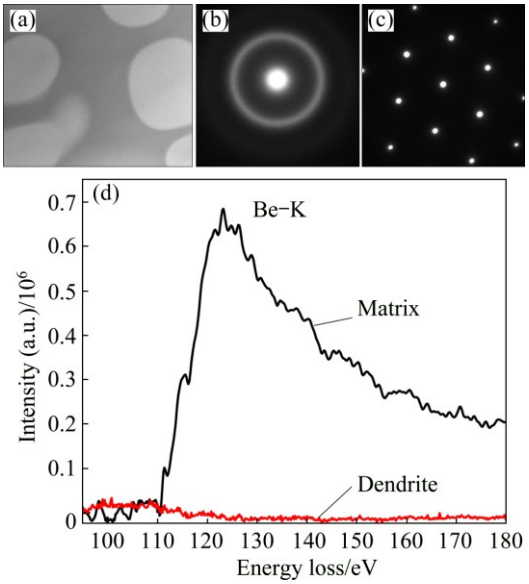


**Fig. 3** Bright-field TEM image of a typical morphology of studied alloy (a), SAED pattern of glassy matrix (b), SAED pattern from [111] zone axis of dendrite (c), background subtracted EELS spectra of Be−K edge as collected from amorphous matrix (black) and from dendrites (red) in Fig. 3(a) (d)

Figure 4(a) shows a high-angle annular dark field (HAADF)−STEM image of the composite, and Figs. 4(b)−(d) show the STEM−EELS compositional maps of Ti, V and Be, respectively. It can be seen that Ti and V are abundant in the dendrites, while Be is exclusively localized in the amorphous matrix, which supports the results shown in Fig. 3.

## 4 Discussion

Compositions of the crystallized dendrites and the amorphous matrix exert influences on the mechanical properties of the composite. In order to determine these compositions, a quantitative method was developed, which was based on the SEM−EDS results shown in Fig. 5.

SEM−EDS analysis shown in Table 1 measures the average composition to be $Ti_{54.5}Zr_{25.7}Cu_{5.9}V_{13.9}$, in comparison to the nominal composition (with the exception of Be) of $Ti_{56.6}Zr_{22.9}Cu_6V_{14.5}$, with the standard deviation under 12.2%. EDS analysis provides the average composition of the amorphous matrix (without Be) and the crystallized dendrite to be $T_{45}Zr_{34.8}Cu_{10.6}V_{9.6}$ and $Ti_{62.4}Zr_{18.4}Cu_{2.6}V_{16.6}$, respectively.

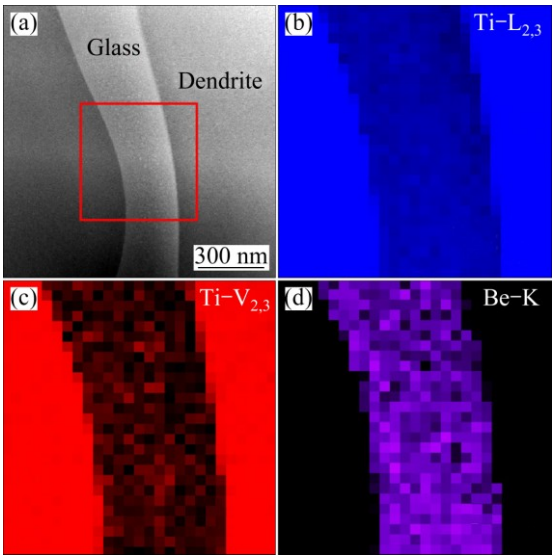


**Fig. 4** HAADF−STEM image of MGMCs (a), and STEM−EELS compositional maps of Ti, V and Be of red area in Fig. 4(a) (b−d)

The second step is to determine the actual composition of the amorphous matrix, by making use of the exclusive presence of Be in the matrix. In order to calculate the composition the matrix, Eqs. (1) (for Be) and (2) (for a heavy element), based on the conservation of atoms, were used:

$$\frac{N\rho V}{M}=\frac{N_{\mathrm{m}}\rho_{\mathrm{m}}V_{\mathrm{m}}}{M_{\mathrm{m}}} \tag{1}$$

$$\frac{N\rho V}{M}=\frac{N_{\mathrm{m}}\rho_{\mathrm{m}}V_{\mathrm{m}}}{M_{\mathrm{m}}}+\frac{N_{\mathrm{d}}\rho_{\mathrm{d}}V_{\mathrm{d}}}{M_{\mathrm{d}}} \tag{2}$$

where $N$, $N_{\mathrm{m}}$ and $N_{\mathrm{d}}$ are the mole fractions of the composite, the amorphous matrix and the dendrites, respectively; $\rho$, $\rho_{\mathrm{m}}$ and $\rho_{\mathrm{d}}$ are densities of the composite, the amorphous matrix and the dendrites, respectively. Since the density of Ti-based Be-containing MGMCs is 4.97−5.13 g/cm$^3$ [29], the density of Ti-Based MG is 4.79−5.12 g/cm$^3$ [28], and the density of the Ti-alloys is 4.3−5.1 g/cm$^3$ [30]. For simplicity, we suggested in this study that $\rho=\rho_{\mathrm{m}}=\rho_{\mathrm{d}}=5.1$ g/cm$^3$. $V$, $V_{\mathrm{d}}$ and $V_{\mathrm{m}}$ are the volume fractions of the composite, the matrix and the dendrites, respectively. The volume fractions of the glass matrix and the dendrites are shown in Fig. 2. $M$, $M_{\mathrm{m}}$ and $M_{\mathrm{d}}$ are the molecular masses of the composite, the matrix and the dendrites, respectively.

In this case, Eqs. (1) and (2) are reduced to:

$$\frac{NV}{M}=\frac{N_{\mathrm{m}}V_{\mathrm{m}}}{M_{\mathrm{m}}} \tag{3}$$

$$\frac{NV}{M}=\frac{N_{\mathrm{m}}V_{\mathrm{m}}}{M_{\mathrm{m}}}+\frac{N_{\mathrm{d}}V_{\mathrm{d}}}{M_{\mathrm{d}}} \tag{4}$$

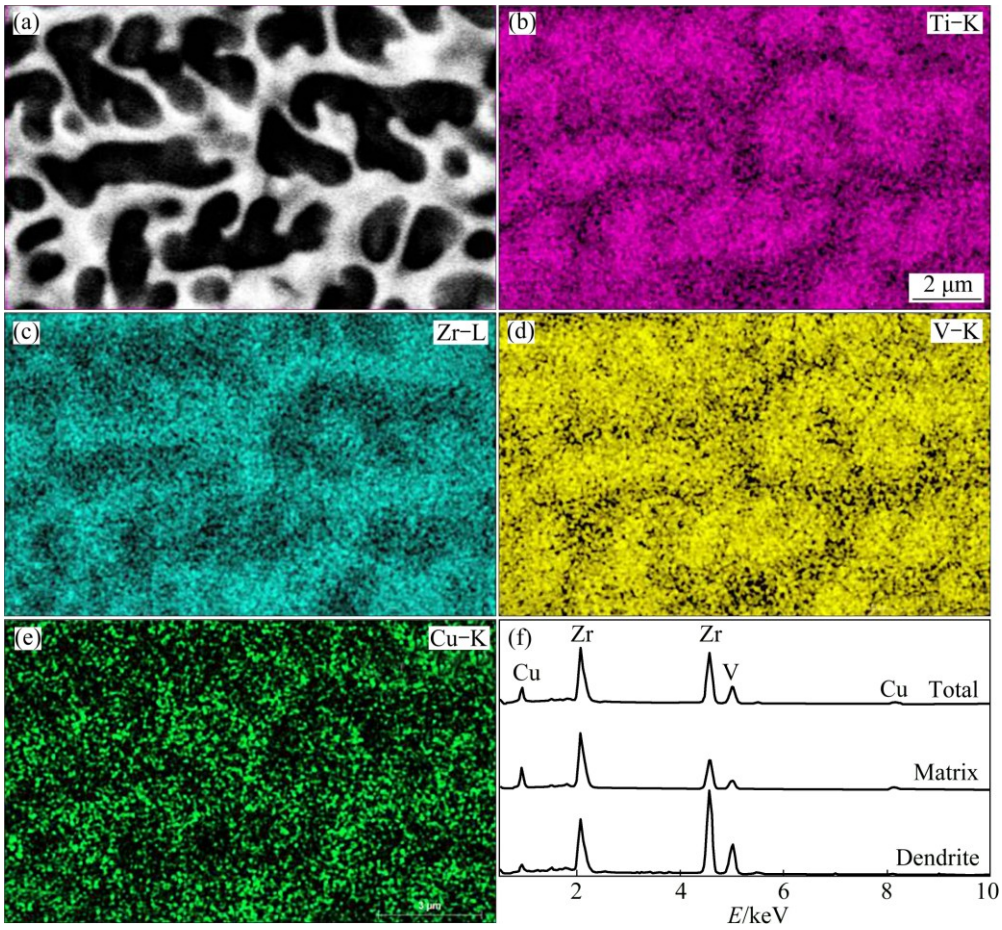


**Fig. 5** SEM−EDS compositional maps: (a) SEM image of MGMCs; (b−e) Corresponding SEM−EDS compositional maps of Ti, Zr, V, and Cu elements, respectively; (f) EDS spectra for whole composite, amorphous matrix and crystalline dendrite, respectively

**Table 1** Average compositions of composite (mole fraction, %)

| Element | Nominal composition/% | EDS mapping/% | Nominal theory barring Be/% | Deviation/% |
|---|---|---|---|---|
| Ti | 47 | 54.5 | 56.6 | 3.7 |
| Zr | 19 | 25.7 | 22.9 | 12.2 |
| Cu | 5 | 5.9 | 6.0 | 1.7 |
| V | 12 | 13.9 | 14.5 | 4.1 |
| Be | 17 | − | − | − |

**Table 2** Summary composition of every phase

| Element | Dendrite EDS/% | Calculated matrix/% | Calculated barring Be-matrix/% | EDS-matrix/% | Deviation/% |
|---|---|---|---|---|---|
| Ti | 62.4 | 28.3 | 45.4 | 45 | 0.8 |
| Zr | 18.4 | 19.7 | 31.6 | 34.8 | 10.9 |
| Cu | 2.6 | 8 | 12.7 | 10.6 | 19.8 |
| V | 16.6 | 6.4 | 10.3 | 9.6 | 7.3 |
| Be | − | 37.6 | − | − | − |

As confirmed by STEM−EELS, Be is only presented in the matrix, which attributes all Be in the nominal composition to the matrix only. Using Eqs. (1)−(4), the average composition of the matrix has been determined to be $Ti_{28.3}Zr_{19.7}Cu_8V_{6.4}Be_{37.6}$ (mole fraction, %) with the standard deviation under 20%. The results are summarized in Table 2. The results are similar to those previously reported in literature [17].

A possible reason for the exclusive distribution of Be in the matrix is as follows. The composite contains five elemental constituents with a large difference in their atomic radii. The atomic radius of Be is relatively small (1.128 Å), compared to those of Cu (1.278 Å), V (1.316 Å), Ti (1.4615 Å), and Zr (1.6025Å) [31]. The difference in the atomic radius can be responsible for the difference in solubility of each element in the crystallized phase. Since the crystalline phases contain a small number of non-equivalent positions in their unit cells, larger fluctuation is required for the nucleation of crystalline phases. So, the relatively small atomic radius of Be helps to increase the atomic packing density of the liquid-like amorphous structures.

From the perspective of thermodynamics, the difference of the Gibbs free energy ($\Delta G$) between the

liquid and the crystalline phases can be expressed as:

$$\Delta G=\Delta H-T\Delta S \quad (5)$$

where $\Delta H$ is the enthalpy of mixing, $T$ is the temperature and $\Delta S$ is the total entropy of fusion. Local atomic structure in liquid phases can be influenced by a small fluctuation of the enthalpy of mixing, which further contributes to the stabilization of the liquid phase. The mixing enthalpy $\Delta H^{mix}$ of Ti−V, Ti−Cu, Ti−Be, Ti−Zr, Zr−V, Zr−Cu, Zr−Be, V−Be, V−Cu, and Cu−Be is −2, −9, −30, 0, −4, −23, −43, −16, 5 and 0 kJ/mol, respectively [32]. The lowest value of Zr−Be mixing enthalpy makes the pair the easiest for amorphous formation. Since the EDS analysis shows that Zr is abundant in the amorphous matrix, we can infer that Be prefers the amorphous matrix due to the small mixing enthalpy of the Zr−Be pair. Our results are consistent with previous reports [33], suggesting that Zr−Be binary alloys are usually amorphous.

## 5 Conclusions

1) The results revealed that the crystal phase is dendritic morphology with good connectivity, the dendritic diameter is 0.5−2 μm, and the inter-dendritic distance is about 300 nm.

2) The volume fractions of the dendrites and amorphous phase are 61.5% and 38.5%, respectively.

3) STEM−EELS has been used to study the Be distribution in MGMCs. The exclusive presence of Be in the amorphous matrix has been revealed.

4) The compositions of both the $Ti_{62.4}Zr_{18.4}Cu_{2.6}V_{16.6}$ dendritic phase and the $Ti_{28.3}Zr_{19.7}Cu_8V_{6.4}Be_{37.6}$ matrix have been determined, which exert significant impacts on improving the mechanical properties of Be-containing MGMCs.

## Acknowledgment

The authors thank Core Facility for Protein Research, CAS for providing the dual-beam FIB/SEM, Yuan JI, Li WANG, Gang JI, Jian-guo ZHANG for EBSD measurement and 3D reconstruction.

## References

[1] DING Shi-yan, LIU Yan-hui, LI Yang-lin, LIU Ze, SOHN S, WALKER F J, SCHROERS J. Combinatorial development of bulk metallic glasses [J]. Nature Materials, 2014, 13(5): 494−500.

[2] GLUDOVATZ B, NALEWAY S E, RITCHIE R O, KRUZIC J J. Size-dependent fracture toughness of bulk metallic glasses [J]. Acta Materialia, 2014, 70: 198−207.

[3] GU Ji, ZHANG Li-xin, WANG Yi-han, NI Song, GUO Sheng-feng, SONG Min. Combined effect of isothermal annealing and pre-compression on mechanical properties of $Cu_{36}Zr_{48}Al_8Ag_8$ bulk metallic glass [J]. Transactions of Nonferrous Metals Society of China, 2016, 26(6): 1620−1628.

[4] GUO H, YAN P F, WANG Y B, TAN J, ZHANG Z F, SUI M L, MA E. Tensile ductility and necking of metallic glass [J]. Nature Materials, 2007, 6(10): 735−739.

[5] WU Hong, LAN Xiao-dong, LIU Yong, LI Fei, ZHANG Wei-dong, CHEN Zi-jin, ZAI Xiong-fei, ZENG Han. Fabrication, tribological and corrosion behaviors ofdetonation gun sprayed Fe-based metallic glasscoating [J]. Transactions of Nonferrous Metals Society of China, 2016, 26(6): 1629−1637.

[6] HUI X, DONG W, CHEN G L, YAO K F. Formation, microstructure and properties of long-period order structure reinforced Mg-based bulk metallic glass composites [J]. Acta Materialia, 2007, 55(3): 907−920.

[7] LEE M L, LI Y, SCHUH C A. Effect of a controlled volume fraction of dendritic phases on tensile and compressive ductility in La-based metallic glass matrix composites [J]. Acta Materialia, 2004, 52(4): 4121−4131.

[8] HU X, NG S C, FENG Y P, LI Y. Glass forming ability and in-situ composite formation in Pd-based bulk metallic glasses [J]. Acta Materialia, 2003, 51(2): 561−572.

[9] HAYS C C, KIM C P, JOHNSON W L. Microstructure controlled shear band pattern formation and enhanced plasticity of bulk metallic glasses containing in situ formed ductile phase dendrite dispersions [J]. Physical Review Letters, 2000, 84(13): 2901−2904.

[10] CHENG J L, CHEN G, XU F, DU Y L, LI Y S, LIU C T. Correlation of the microstructure and mechanical properties of Zr-based in-situ bulk metallic glass matrix composites [J]. Intermetallics, 2010, 18(12): 2425−2430.

[11] QIAO J W, ZHANG Y, JIA H L, YANG H J, LIAW P K, XU B S. Tensile softening of metallic-glass-matrix composites in the supercooled liquid region [J]. Applied Physics Letters, 2012, 100(12): 121902−4.

[12] QIAO Jun-wei. In-situ dendrite/metallic glass matrix composites: A review [J]. Journal of Materials Science & Technology, 2013, 29(8): 685−701.

[13] QIAO J W, ZHANG T, YANG F Q, LIAW P K, PAULY S, XU B S. A tensile deformation model for in-situ dendrite/metallic glass matrix composites [J]. Scientific Reports, 2013, 3: 2816.

[14] HOFMANN D C, SUH J Y, WIEST A, DUAN G, LIND M L, DEMETRIOU M D, JOHNSON W L. Designing metallic glass matrix composites with high toughness and tensile ductility [J]. Nature, 2008, 451(7182): 1085−1089.

[15] KIM C P, SUH J Y, WIEST A, LIND M L, CONNERC R D, JOHNSON W L. Fracture toughness study of new Zr-based Be-bearing bulk metallic glasses [J]. Scripta Materialia, 2009, 60(2): 80−83.

[16] WANG Yong-sheng, GUO Zhen-xi, MA Rui, HAO Guo-jian, ZHANG Yong, LIN Jun-pin, SUI Man-ling. Investigation of the microcrack evolution in a Ti-based bulk metallic glass matrix composite [J]. Progress in Natural Science: Materials International, 2014, 24(2): 121−127.

[17] QIAO J W, SUN A C, HUANG E W, ZHANG Y, LIAW P K, CHUANG C P. Tensile deformation micromechanisms for bulk metallic glass matrix composites: From work-hardening to softening [J]. Acta Materialia, 2011, 59(10): 4126−4137.

[18] WANG Y S, HAO G J, QIAO J W, ZHANG Y, LIN J P. High strain rate compressive behavior of Ti-based metallic glass matrix composites [J]. Intermetallics, 2014, 52: 138−143.

[19] JANKOWSKI A F, WALL M A, van BUUREN A W, NIEH T G, WADSWORTH J. From nanocrystalline to amorphous structure in beryllium-based coatings [J]. Acta Materialia, 2002, 50(19): 4791−4800.

[20] HANG X F, WANG X D, KIM K B, YI S. Be effect on glass-forming ability and mechanical properties of Ti−Cu−Co−Zr−Sn bulk metallic glasses [J]. Materials Transactions, 2006, 47(9): 2321−2325.

[21] PEKER A, JOHNSON W L. A highly processable metallic glass: $Zr_{41.2}Ti_{13.8}Cu_{12.5}Ni_{10.0}Be_{22.5}$ [J]. Applied Physics Letters, 1993, 63(17): 2342−2344.
[22] HOFMANN D C. Shape memory bulk metallic glass composites [J]. Science, 2010, 329: 1294−1295.
[23] OH Y S, KIM C P, LEE S, KIM N J. Microstructure and tensile properties of high-strength high-ductility Ti-based amorphous matrix composites containing ductile dendrites [J]. Acta Materialia, 2011, 59(19): 7277−7286.
[24] WANG Y S, HAO G J, ZHANG Y, LIN J P, QIAO J W. Fabrication and mechanical characterization of Ti-based metallic glass matrix composites by the Bridgman solidification [J]. Metallurgical and Materials Transactions A, 2014, 45(5): 2357−2362.
[25] CHEN P, MAO S C, LIU Y, WANG F, ZHANG Y F, ZHANG Z, HAN X D. In-situ EBSD study of the active slip systems and lattice rotation behavior of surface grains in aluminum alloy during tensile deformation [J]. Materials Science & Engineering A, 2013, 580: 114−124.
[26] GUO S F, LIU L, LI N, LI Y. Fe-based bulk metallic glass matrix composite with large plasticity [J]. Scripta Materialia, 2010, 62(6): 329−332.
[27] HE G, LÖSER W, ECKERT J. Enhanced plasticity in a Ti-based bulk metallic glass-forming alloy by in situ formation of a composite microstructure [J]. Journal of Materials Research, 2002, 17(12): 3015−3018.
[28] HOFMANN D C, SUH J Y, WIEST A, LIND M L, DEMETRIOU M D, JOHNSON W L. Development of tough, low-density titanium-based bulk metallic glass matrix composites with tensile ductility [J]. Proceedings of the National Academy of Sciences, 2008, 105(51): 20136−20140.
[29] PARK J M, KIM Y C, KIM W T, KIM D H. Ti-based bulk metallic glasses with high specific strength [J]. Materials Transactions, 2004, 45(2): 595−598.
[30] TELFORD M. The case for bulk metallic glass [J]. Materials Today, 2004, 7: 36−43.
[31] SENKOV O N, MIRACLE D B. Effect of the atomic size distribution on glass forming ability of amorphous metallic alloys [J]. Materials Research Bulletin, 2001, 36(12): 2183−2198.
[32] TAKEUCHI A, INOUE A. Classification of bulk metallic glasses by atomic size difference, heat of mixing and period of constituent elements and its application to characterization of the main alloying element [J]. Materials Transactions, 2005, 46(12): 2817−2829.
[33] TANNER L E, RAY R. Metallic glass formation and properties in Zr and Ti alloyed with Be—I the binary Zr−Be and Ti−Be systems [J]. Acta Metallurgica,1979, 27(11): 1727−1747.

# 含 Be 非晶复合材料中 Be 元素的分布

郭振玺[1,2]，王永胜[3,4]，朱陆军[1]，张跃飞[1]，张振华[1]，
柯小行[1]，林均品[4]，郝国建[4]，张 泽[1,5]，隋曼龄[1]

1. 北京工业大学 固体微结构与性能研究所，北京 100124；
2. 中国科学院生物物理研究所 蛋白质科学研究平台生物成像中心，北京 100101；
3. 太原理工大学 材料科学与工程学院，太原 030024；
4. 北京科技大学 新材料国家重点实验室，北京 100083；
5. 浙江大学 材料科学与工程学系，硅材料国家重点实验室，杭州 310027

**摘 要**：采用 XRD、SEM、EBSD、TEM、EDS 以及三维组织重构方法系统研究原位 Be 元素的 Ti 基非晶复合材料 $Ti_{47}Zr_{19}Cu_5V_{12}Be_{17}$(摩尔分数，%)中晶体相的形态、尺寸、成分和体积分数，并采用 STEM−EELS 证明 Be 元素仅仅分布在非晶基体中。在此基础上，准确地得到了晶体相和非晶基体的化学成分分别为 $Ti_{62.4}Zr_{18.4}Cu_{2.6}V_{16.6}$ 和 $Ti_{28.3}Zr_{19.7}Cu_8V_{6.4}Be_{37.6}$(摩尔分数，%)，相应的体积分数分别为 61.5%和 38.5%, 该结果对设计原位含 Be 非晶复合材料具有重要的指导意义。

**关键词**：非晶；复合材料；微观结构；电子能量损失谱；Be 元素分布

**(Edited by Yun-bin HE)**